IEEE Photonics Journal
An IEEE Photonics Society Publication

Open Access

Maxwell Fish-Eye and Half-Maxwell Fish-Eye Based on Graded Photonic Crystals

Volume 10, Number 3, June 2018

Fabian Gaufillet
Eric Akmansoy

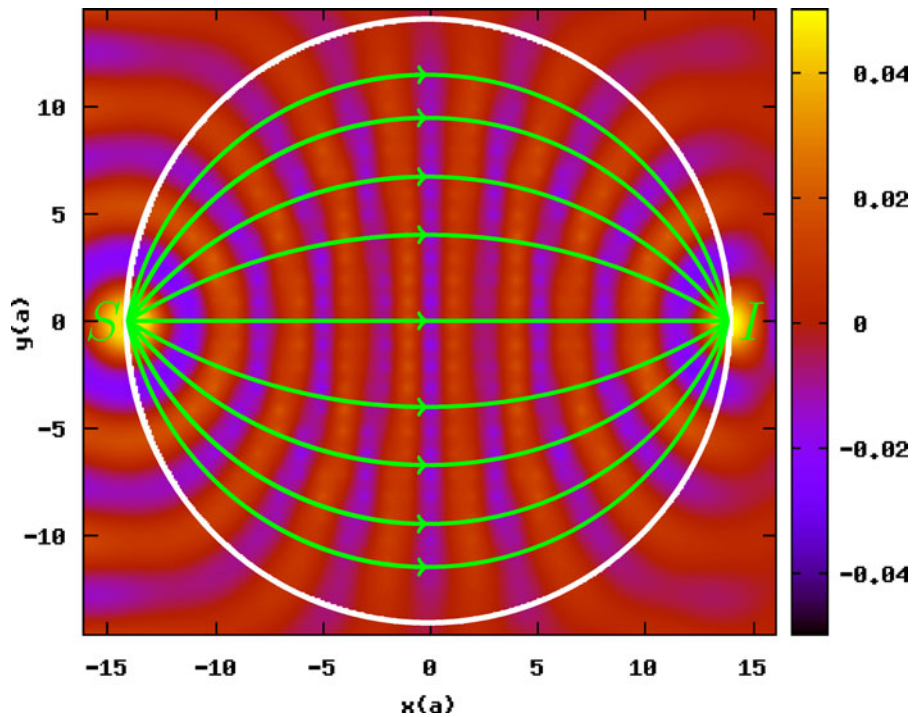

DOI: 10.1109/JPHOT.2018.2835157
1943-0655 © 2018 IEEE

IEEE photonics SOCIETY

IEEE

Maxwell Fish-Eye and Half-Maxwell Fish-Eye Based on Graded Photonic Crystals

Fabian Gaufillet and Eric Akmansoy

Institut d'Électronique Fondamentale, Univ. Paris-Sud, Université Paris-Saclay, Orsay F-91405, France, and UMR8622, CNRS, Orsay F-91405, France

DOI:10.1109/JPHOT.2018.2835157

Manuscript received April 19, 2018; accepted May 4, 2018. Date of publication May 21, 2018; date of current version June 8, 2018. Corresponding author: Eric Akmansoy (e-mail: eric.akmansoy@u-psud.fr).

Abstract: We report on the design of the Maxwell fish-eye based on graded photonic crystals. It is a radially graded refractive index structure, whose remarkable property is to form perfect images in the sense of geometrical optics. The half-Maxwell fish-eye, which takes advantage of the symmetry of the previous, provides directive emission, which applies, amongst others, to wireless communications. The continuous gradient index is nevertheless difficult to practically realize. We show that graded photonic crystals make it possible to get the radially graded index of the Maxwell fish-eye and that the designed graded photonic crystals exhibit the expected properties. Graded photonic crystals fit the requirements of graded index optics. Moreover, they can be scaled with the wavelength.

Index Terms: Maxwell fish-eye, half-Maxwell fish-eye, gradient-index optics, photonic crystals, optical coupling components, lens-antennas.

1. Introduction

The Maxwell Fish-Eye (MFE) is a spherically symmetric graded index structure which has the remarkable property of forming perfect images in the geometrical optics point of view [1, chap. 4]. This isotropic medium of variable refractive index is called an absolute instrument [2], [3]. The Half-Maxwell Fish-Eye (HMFE) takes advantage of the symmetry of the MFE. It is thus half the MFE, i.e. a hemisphere, and it is a useful device because it exhibits directive emission when, e.g., it is fed by an antenna. Indeed, it collimates a source point located on the spherical surface into a directive plane wave whose aperture is that of the lens. Conversely, it focuses an incident plane wave onto its spherical surface. Luneburg [4] and Eaton [5] lenses are the other known examples of absolute instruments [3]. Miñano refined this definition introducing "Novel Absolute Instruments for Homogeneous Regions", that is, a class of spherically symmetric gradient-index structures forming a perfect image such that the object and the image lie in regions of the same constant refractive index [6]. In a prominent paper, Pendry gave the evidence of the perfect lens with negative refraction index ($n = -1$), by showing this medium amplifies the evanescent waves, which causes both propagating and evanescent waves to contribute to the resolution of the image [7]. The question next arose as to whether positive index absolute instruments in the geometrical optics sense were also perfect instruments in the wave optics sens, i.e., are they also diffraction unlimited? Ma *et al.* have argued that the mirrored MFE gives unlimited resolution [8]; these results were the

matter of a serious debate (see e.g., [9]–[11]) and were subsequently retracted. MFE thereby blends tricky theoretical aspects with efficacious applications.

GRaded INdex (GRIN) Optics is undergoing a renewal because the "possibility of realising arbitrary refractive index profiles opens up prospects for optical design" [12], [13]. The refractive index of a GRIN lens depends on the location inside it, which offers new degrees of freedom for optical design. Because of the tailored graded index, the optical rays are curved and GRIN optics reduces the size and the complexity of lens assemblies. GRIN optical components for coupling and interconnects in photonic systems are thus designed [14]. Nevertheless, the continuous gradient of index is difficult to realize in practice. The graded index profile is often discretized by stacking concentric shells of various permittivity [15]–[17]. It has also been obtained by varying the distance between the two circular metal plates of a waveguide-based artificial dielectric [18], or by controlling the thickness of a guiding Silicon layer [19], [20]. Herein, we propose to attain the radially graded refractive index of the MFE *via* the continuous gradient of filling factor of Graded Photonic Crystals (GPC). The graded index $n(r)$ of the Maxwell Fish-Eye is therefore not discretized. Contrary to metamaterials, it involves no resonance of the constitutive medium [21] and the losses are consequently negligible, the latter affecting the resolution. In addition, as GPCs may be fabricated by various processes, including nanolithography (e.g. by implementing the Silicon-on-insulator technology, that is compatible with CMOS circuits), they can be designed and fabricated for applications from microwave to the optical domain. GPCs, with their fabrication techniques, are the materials to a new approach of GRIN optics. Compact opticals devices at scale of a few wavelengths are provided this way.

MFE index profile varies from the center towards the rim according to the relation

$$n(r) = \frac{2}{1 + (r/R)^2}, \tag{1}$$

where r is the radial distance inside the structure region and R is the radius of the structure. Its refractive index therefore varies from $n(0) = 2$ to $n(R) = 1$, and it does not depend on the other coordinates. When $r = R$, it is half of its value at the center of the MFE. It images each point located on the spherical surface of radius R to the opposite point on the same surface. Two such points, object and image, are said to be perfect conjugates. This optical system is stigmatic, whereby all the optical rays emerging from the object converge onto the same unique image and inside the structure, the paths of the rays are along arcs of circles [1, chap. 4]. The principle of Maxwell Fish-Eye is shown in Fig. 1. Maxwell Fish-Eye has also been treated in the framework of Maxwell equations [22].

We attain the radially graded index $n(r)$ of the Maxwell Fish-Eye *via* the continuous gradient of the effective index n_{eff} of a GPC, which results from its gradient of filling factor η. The method of design consists in the engineering of the iso-frequency curves (IFC) of photonic crystals (PC). These are artificial media, whose dielectric constant is periodic, which makes their relation of dispersion $\omega = \omega(\mathbf{k})$ to be as a band-structure, i.e. it includes photonic band-gaps and photonic bands. The dispersive properties we handle to design the structures are beyond the photonic band gaps of the band-structure. Indeed, PCs permit to control the flow of the EM field *via* the shape of their photonic bands which relates the group velocity $\mathbf{v_g}$ to the wave vector $\mathbf{k}$, according to the relation [23]

$$\mathbf{v_g} = \nabla_{\mathbf{k}}\omega(\mathbf{k}). \tag{2}$$

The wave vector $\mathbf{k}$ is consequently perpendicular to the iso-frequency curves (IFC); the latter are the relation of dispersion $\omega = \omega(\mathbf{k})$ at a given frequency [23]. IFCs may have a great variety of shapes. If these are circular shapes, the PC can be assumed to behave as a homogeneous isotropic medium and an isotropic effective index n_{eff} can be retrieved [23].

For their part, Graded Photonic Crystals rely on the small variation of one parameters of the elementary cell, such as the filling factor or the lattice period, over one period of the lattice of the PC [24]. Since this variation is small over the elementary cell of the PC, the dispersive properties of GPCs can be deduced from that of PCs. This small variation gradually modifies the dispersion properties. Consequently, engineering the IFCs allows to really control the direction of the wave

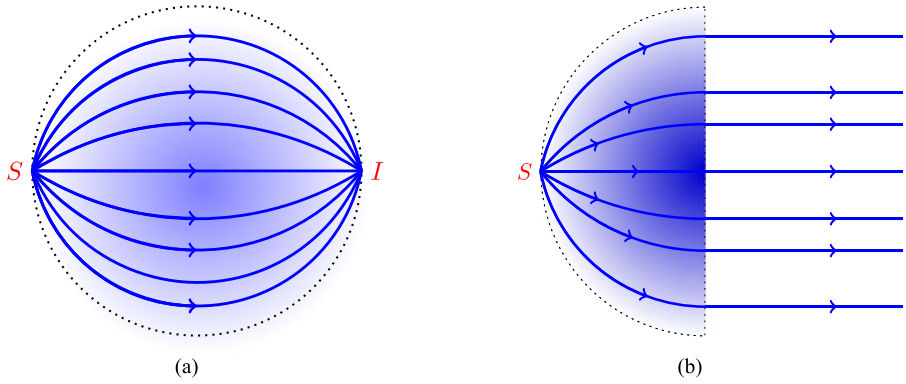

Fig. 1. Optical paths in Maxwell Fish-Eye and Half-Maxwell Fish-Eye. These are Graded Index optical components, in which the optical paths are not along straight lines. Indeed, as the index depends on the position inside with gradual variations, these are curved. The graded index $n(r)$ of the Maxwell Fish-Eye is radially varying. (a) Maxwell Fish-Eye: its index follows eq. (1), i.e., its value at the center is twice the value at its rim. All the rays emerging from the point source S are converging onto the image point I, the latter being the symmetric of the former. The optical paths are along arcs of circles and the wave fronts are consequently symmetric. (b) The Half-Maxwell Fish-Eye is half the Maxwell Fish-Eye, that is, it is an hemisphere. It takes advantage of this symmetry, e.g., all the rays emitted by the point source S emerge as a parallel beam. Conversely, it focuses an incident plane wave onto its spherical surface.

vector **k**. GPCs have been therefore a step forward to control the propagation of the EM field [24] since their effectiveness to curve the flow of light as been demonstrated [25]–[27].

2. Design and Simulation of the Maxwell Fish-Eye

2.1 Effective index

In this paper, we consider structures which are derived from PCs whose dispersive properties make them analogous to Linear, Homogeneous and Isotropic (LHI) media. A gradient is applied to the elementary cell giving rise to the GPC. To design the latter, we vary the filling factor η, each elementary cell of the GPC being square. At the operating frequency, the dispersion relation corresponding to each elementary cell is thus circular. Consequently, at the scale of the elementary cell, the GPC can be seen as a homogeneous and isotropic medium, although the whole structure is an inhomogeneous medium. In addition, at the interface of the photonic crystal with vacuum, the tangential component of the wave vector **k** is continuous. These are the two key points to design a GRIN structure from a GPC.

We address a 2D GPC, that is, a square lattice of circular dielectric cylinders ($\epsilon_r = 8.9$) embedded in air ($\epsilon_r = 1$); a schematic layout is shown in Fig. 2. Its radius is $R = 3\lambda \simeq 14.3 \times a$ and the filling factor η is

$$\eta = \frac{\pi \times \phi^2}{4 \times a^2}, \tag{3}$$

where ϕ is the diameter of the constitutive dielectric cylinders and a is the period of the square lattice. To design the GPC, the diameter ϕ is thus varied, whereas the lattice period a is constant. We calculate the band structure and the IFCs for different values of the filling factor η by the means of our "homemade" Finite Difference Time Domain (FDTD) source code which describes the elementary cell with Periodic Boundaries Conditions [28]–[33]. The polarization of the incident wave is transverse magnetic (TM), the electric field being parallel to the axis of the dielectric cylinders. The operating normalized frequency is $\varpi = a/\lambda = 0.21$. Extremal band-structures are reported in Fig. 3, corresponding to the smallest diameter of the cylinders and to the greatest diameter of the cylinders.

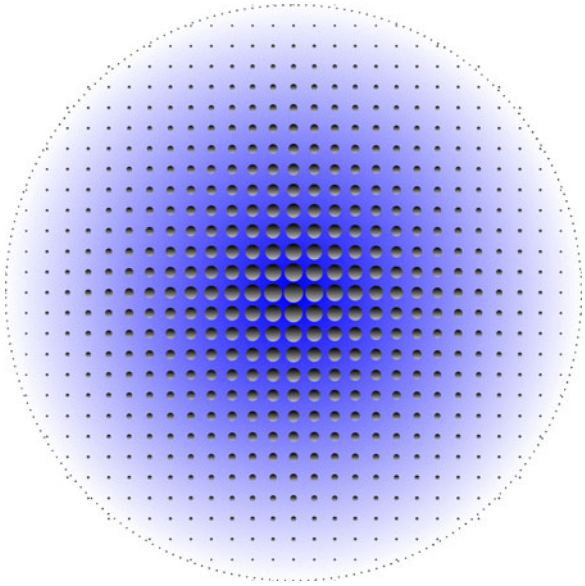

Fig. 2. Schematic layout of the GPC. The circular dielectric cylinders are arranged in a square lattice. Their diameter, and consequently the filling factor η, decreases from the center of the GPC towards its rim; and also decreases the effective index n_{eff}.

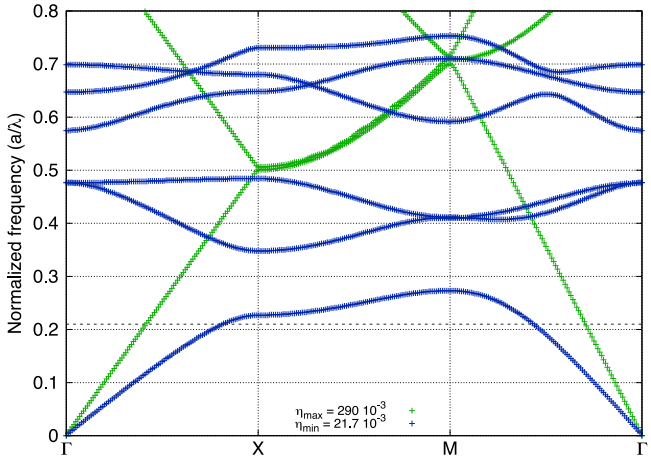

Fig. 3. Band structures of two 2D dielectric PCs made of circular cylinders arranged in a square lattice corresponding to the extremal values of the filling factor η. The diameter of the cylinders of each PC is constant. The green curve corresponds to the smallest diameter of the cylinders of the GPC, while the blue one corresponds to the greatest diameter of the cylinders. The incident electric field is parallel to the axis of the cylinders (TM polarization). The horizontal dashed line indicates the operating normalized frequency $\varpi = 0.21$. The filling factor varies from $\eta = 21.7 \cdot 10^{-3}$ to $\eta = 290 \cdot 10^{-3}$.

Taking benefit from the continuity of the tangential component of the wave vector **k**, we calculate the effective index n_{eff} from the ratio of the radius of the IFCs to that of the relation of dispersion of the vacuum; the latter is generally called the "light cone" [23]. Several IFCs corresponding to various filling factors and the "light cone" are shown in Fig. 4; they are nearly circular. The side of the square mesh cell of the FDTD grid is $dx = a/100$, which may impact the resolution meshing when dicretizing the cylinders.

As the diameter of the cylinder increases, the effective index n_{eff} increases. Thereby, we deduce a "calibration curve" $n_{eff} = n_{eff}(\eta)$, that is, the variation of the effective index n_{eff} in function of the filling

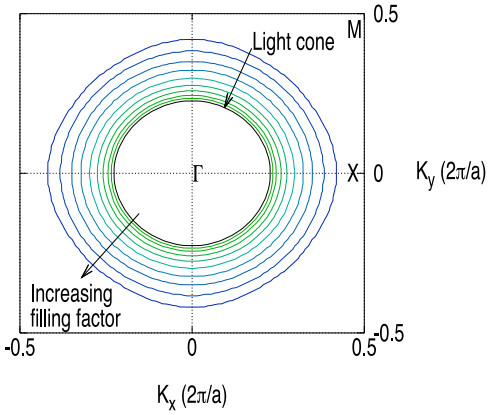

Fig. 4. Several isofrequency curves (TM polarization) for increasing filling factor η and that of vacuum (black curve), the latter being referred to as the "light cone". Each of these curves is nearly circular. The filling factor varies from $\eta = 15.4 \cdot 10^{-3}$ to $\eta = 256 \cdot 10^{-3}$. The operating normalized frequency is $\varpi = a/\lambda = 0.21$.

factor η: the former increases with the latter. Thanks to this calibration curve $n_{eff}(\eta)$, we extrapolate the different diameters of the constitutive cylinders of the GPC, so as to fit the index profil $n(r)$ of the MFE (eq. 1). As expected, these decrease from the center of the Maxwell Fish-Eye towards its rim (Fig. 2). Note that varying one parameter of the elementary cell, i.e., the lattice period a, the filling factor η or the dielectric constant ϵ_r, makes it possible to fit any arbitrary profile of refractive index for GRIN optics design.

Retrieving the effective index n_{eff} from the radius of the IFCs is suitable for any photonic band in the band structure, having a positive or a negative curvature. It does not depend on the normalized frequency $\varpi = a/\lambda$. To handle an isotropic medium only requires circular IFCs at the operating frequency ϖ, the PC being dielectric or metallic [30]–[33]. It therefore deals with the true relation of dispersion of PCs. It is applicable from microwave to the optical range, e.g., it is applicable to the design of a PC slab between two different media such as $air/Si/SiO_2$. Note that the gradient of filling factor η depends on the radial r and polar θ coordinates r (Fig. 2) unlike the refractive index $n(r)$ of the Maxwell Fish-Eye which only depends on the radial coordinate.

2.3 Simulation of the Maxwell Fish-Eye

Once designed, we simulate the MFE by the means of our FDTD code, which involves Perfectly Matched Layer boundaries conditions and the Total Field/Scattered Field method [30]–[34]. Simulations are carried out at the normalized frequency $\varpi = 0.21$, the source point being located on the surface of the MFE. The result of the simulation is reported in Fig. 5: the source point is set on the left and the EM field propagates along the $\Gamma - X$ direction of the GPC. The object is really imaged on the opposite side of the structure, while the wavefronts are inside symmetric regarding the plane of symmetry between the object and the image; whereby the inside optical rays emerging from the source point converge onto the same image point. We also set the source point so that the EM field propagates along the $\Gamma - M$ direction of the GPC. The object is similarly imaged on the opposite side of the structure, while the wavefronts exhibit the same symmetry (result not shown). Our GPC clearly achieves the properties of the MFE.

3. Half-Maxwell Fish-Eye

The HMFE takes advantage of this symmetry. We consider both the collimation and the focusing properties of the HMFE and the corresponding results are reported in Figs. 6 and 7, respectively. The EM field emitted by a source point on the spherical surface propagates through the lens and

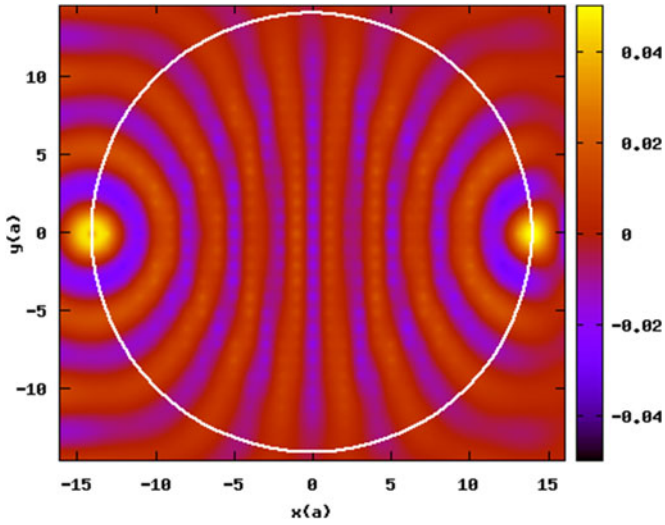

Fig. 5. Map of the instantaneous electric field E_z at the normalized frequency $\varpi = 0.21$ issued from a source point located at the Maxwell Fish-Eye surface (left). It is imaged onto the surface of the MFE on the opposite side (right), i.e. the two points are conjugated, while the inside wavefronts are symmetric. The x direction is along the $\Gamma - X$ direction of the GPC. The radius is $R = 3\lambda$.

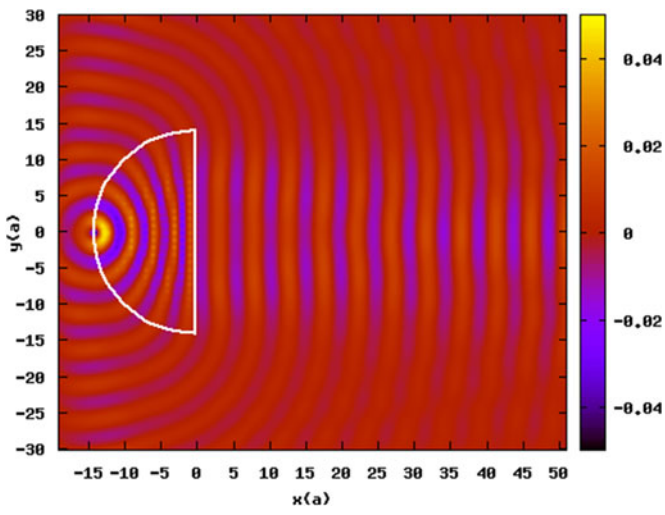

Fig. 6. Map of the instantaneous field E_z at the normalized frequency $\varpi = 0.21$ issued from a source point located at the Half-Maxwell Fish-Eye surface. It is collimated as it emerges from the HMFE and its width is about the aperture of the lens. The radius of the hemisphere is $R = 3\lambda$. The wave propagates along the $\Gamma - X$ direction of the GPC.

the wavefronts of the collimated beam which is emerging from the HMFE are that a plane wave whose width is about the aperture of the HMFE (Fig. 6). Notice the only four wavelengths inside the HME. Collimating by the HMFE may be implemented in infrared wireless telecommunication systems. Then, the HMFE is illuminated by a plane wave incident on its plane side, with a gaussian transverse amplitude: it is clearly focused onto the other side (Fig. 7). Both results demonstrate the ability of GPC to control the "flow of light" in only a few wavelengths.

Since its refractive index radially changes, the lens undergoes spherical aberrations and the focal spot is consequently not a point [35]. The shape of the beam in the focal plane is reported in Fig. 8: it is like a cardinal sine and its Full Width at Half Maximum is $FWHM \simeq 0.35\ \lambda$, which is less than the

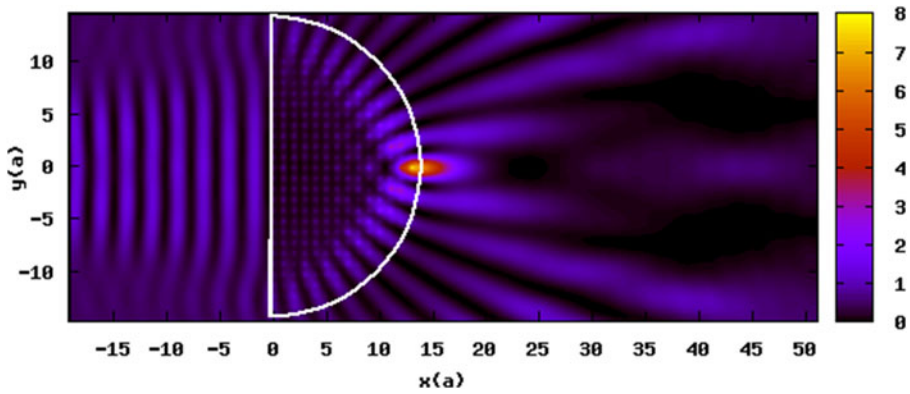

Fig. 7. Map of the mean value of the square of the electric field $\overline{\mathbf{E}_z^2}$ of an incident TM plane wave at the normalized frequency $\varpi = 0.21$ on the Half-Maxwell Fish-Eye. The focus spot is onto the surface of the Half-Maxwell Fish-Eye on opposite side of the incident plane wave which propagates along the x direction. The radius of the hemisphere is $R = 3\lambda$.

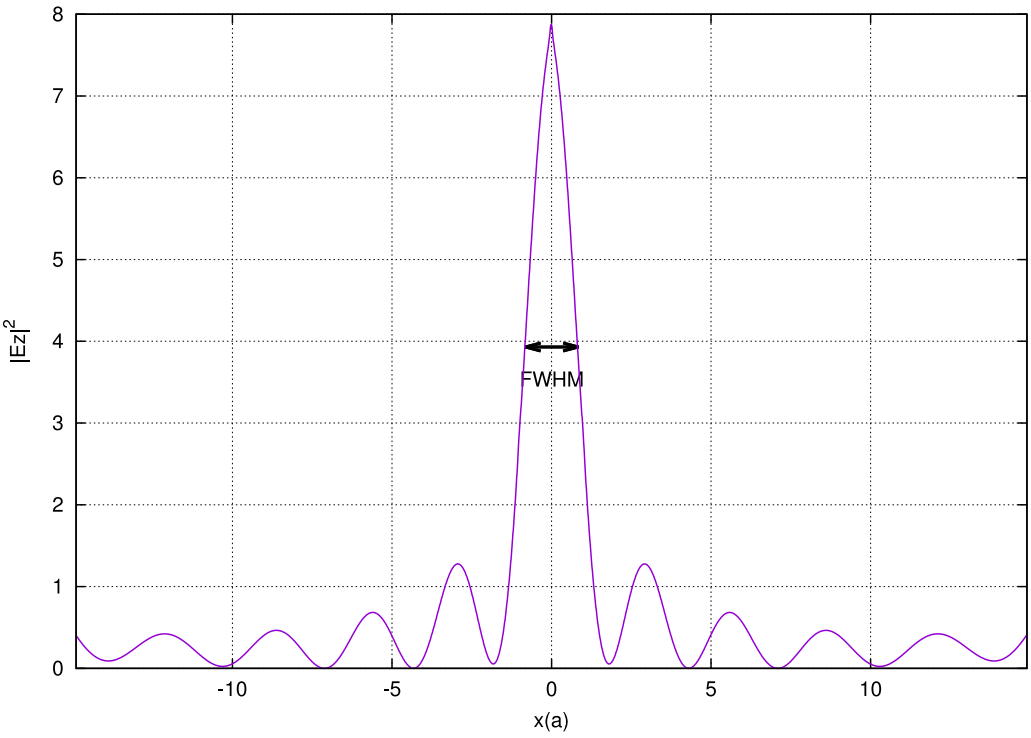

Fig. 8. Shape of the mean value of the square of the electric field $\overline{\mathbf{E}_z^2}$ in the focal plane at the normalized frequency $\varpi = 0.21$.

wavelength.[1] We ascribe this result to the coexistence of propagating waves and evanescent waves at the output interface of the GPC. Luo *et al.* have demonstrated that resolution arbitrarily smaller than the wavelength should be possible in a positive-index photonic crystal, when the lattice period a is much smaller than the operating wavelength [36]. Indeed, they have shown that the evanescent waves can be greatly amplified through transmission because of the coupling between the incident

[1]Another simulation halving the mesh cell of the FDTD grid yielded the same result.

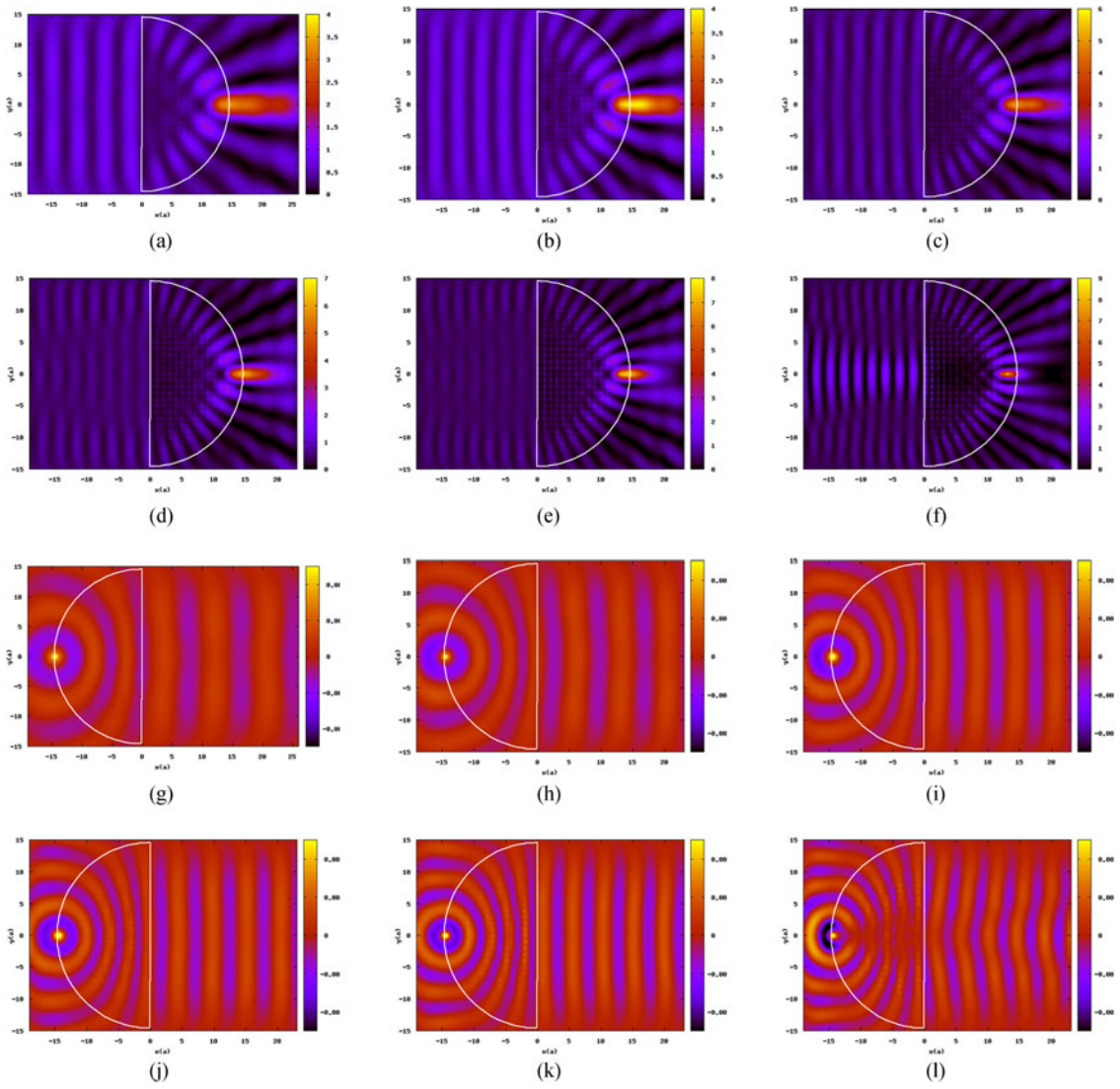

Fig. 9. Operating frequency band of the Half-Maxwell Fish-Eye. (a) to (f): focusing (the operating reduced frequency is in order $\varpi = 0.12, 0.14, 0.16, 0.18, 0.21, 0.23$); (g) to (l) collimation (same values of the operating frequency).

evanescent field and bound photon states which usually exist below the light cone. This contributes to the resolution of the image. Resolution lower than 0.5λ is achievable provided the dielectric constant of the cylinders is high enough. Our GPC satisfies Luo *et al.*' criteria: the lattice period a of our GPC is much smaller than the operating wavelength λ, the contrast of the dielectric constants is 8.9, and the operating frequency ϖ is set in the first photonic band, i.e. under the light cone. Note that the FDTD mesh cell is again $dx = a/100$ in the simulation, which impacts the discretization of the constitutive rods by the square mesh cell of the FDTD grid and brings about approximations in the results of the simulation. HMFE focusing could be implemented for coupling in integrated photonic components.

We also study the operating frequency band and results corresponding to $\varpi = 0.12, 0.14, 0.16, 0.18, 0.21, 0.23$ are reported in Fig. 9. They anew validate previous results, i.e., despite its smallness, the GPC governs the optical paths in a few wavelengths.

4. Conclusion

We designed a GPC whose fitted gradient of filling factor achieves the optical properties of the Maxwell Fish-Eye. The gradient of filling factor has been deduced by engineering the IFCs of PCs. The simulation reveals that the source point and the image point are clearly conjugated, and that the paths of the rays inside the structure are symmetrical. Then, we simulated half the GPC and found its optical properties are that of the Half-Maxwell Fish-Eye, i.e., it provides a directive collimated beam from a source point. Moreover, it conversely focuses an incident plane wave and the spot size is less than one wavelength. These results reveal that GPC are able to govern the flow of the EM field in a few units of wavelengths. These structures are suitable for integrated photonics, lab-on-chip components, wireless communications, antennas systems, from microwave to optics. These ultra-compact GPCs at the scale of the wavelength permit to fit the continuous graded index of the Maxwell Fish-Eye and actually, any graded index profile. GPCs are the means to GRIN optics to expand, from microwave to the optical frequency domain.

References

[1] M. Born and E. Wolf, *Principles of Optics*, 7th ed. Cambridge, U.K: Cambridge Univ. Press, 1999.
[2] J. L. Synge, "The absolute optical instrument," *Trans. Amer. Math. Soc.*, vol. 44, no. 1, pp. 32–46, 1938. [Online]. Available: http://www.jstor.org/stable/1990104.
[3] T. Tyc, L. Herzánová, M. Šarbort, and K. Bering, "Absolute instruments and perfect imaging in geometrical optics," *New J. Phys.*, vol. 13, no. 11, Art no. 115004, 2011.
[4] S. P. Morgan, "General solution of the luneberg lens problem," *J. Appl. Phys.*, vol. 29, no. 9, pp. 1358–1368, 1958.
[5] J. Eaton, "On spherically symmetric lenses," *Trans. IRE Prof. Group Antennas Propag.*, vol. 4, pp. 66–71, Dec. 1952.
[6] J. C. Miñano, "Perfect imaging in a homogeneous three-dimensional region," *Opt. Exp.*, vol. 14, no. 21, pp. 9627–9635, Oct. 2006.
[7] J. B. Pendry, "Negative refraction makes a perfect lens," *Phys. Rev. Lett.*, vol. 85, pp. 3966–3969, Oct. 2000. [Online]. Available: https://link.aps.org/doi/10.1103/PhysRevLett.85.3966.
[8] Y. G. Ma, S. Sahebdivan, C. K. Ong, T. Tyc, and U. Leonhardt, "Evidence for subwavelength imaging with positive refraction," *New J. Phys.*, vol. 13, no. 3, Art no. 033016, 2011. [Online]. Available: http://stacks.iop.org/1367–2630/13/i=3/a=033016.
[9] R. Merlin, "Maxwell's fish-eye lens and the mirage of perfect imaging," *J. Opt.*, vol. 13, no. 2, Art no. 024017, 2011. [Online]. Available: http://stacks.iop.org/2040–8986/13/i=2/a=024017.
[10] R. J. Blaikie, "Perfect imaging without refraction?" *New J. Phys.*, vol. 13, no. 12, p. 125006, 2011.
[11] M. A. Alonso, "Is the Maxwell–shafer fish eye lens able to form super-resolved images?" *New J. Phys.*, vol. 17, no. 7, Art no. 073013, 2015.
[12] P. Milojkovic, S. Tompkins, and R. Athale, "Special section guest editorial: Gradient index optics," *Opt. Eng.*, vol. 52, no. 11, pp. 112 101–112 101, 2013. [Online]. Available: http://dx.doi.org/10.1117/1.OE.52.11.112101.
[13] J. Teichman, J. Holzer, B. Balko, B. Fisher, and L. Buckley, "Gradient index optics at darpa," Defense Adv. Res. Projects Agency, Alexandria, VA, USA, Tech. Rep. D-5027, Nov. 2013.
[14] C. Gomez-Reino, M. Perez, C. Bao, and M. Flores-Arias , "Design of grin optical components for coupling and interconnects," *Laser Photon. Rev.*, vol. 2, no. 3, pp. 203–215, 2008. [Online]. Available: http://dx.doi.org/10.1002/lpor.200810002.
[15] L. C. Gunderson and G. T. Holmes, "Microwave luneburg lens," *Appl. Opt.*, vol. 7, no. 5, pp. 801–804, May 1968. [Online]. Available: http://ao.osa.org/abstract.cfm?URI=ao-7–5-801.
[16] G. Peeler and H. Coleman, "Microwave stepped-index luneberg lenses," *IRE Trans. Antennas Propag.*, vol. 6, no. 2, pp. 202–207, 1958.
[17] B. Fuchs, O. Lafond, S. Rondineau, and M. Himdi, "Design and characterization of half Maxwell fish-eye lens antennas in millimeter waves," *IEEE Trans. Microw. Theory Tech.*, vol. 54, no. 6, pp. 2292–2300, Jun. 2006.
[18] J. Liu, R. Mendis, and D. M. Mittleman, "A Maxwell's fish eye lens for the terahertz region," *Appl. Phys. Lett.*, vol. 103, no. 3, Art no. 031104, 2013. [Online]. Available: https://doi.org/10.1063/1.4813820.
[19] L. H. Gabrielli and M. Lipson, "Integrated luneburg lens via ultra-strong index gradient on silicon," *Opt. Exp.*, vol. 19, no. 21, pp. 20 122–20 127, Oct. 2011. [Online]. Available: http://www.opticsexpress.org/abstract.cfm?URI=oe-19–21-20122.
[20] A. D. Falco, S. C. Kehr, and U. Leonhardt, "Luneburg lens in silicon photonics," *Opt. Exp.*, vol. 19, no. 6, pp. 5156–5162, Mar. 2011.
[21] Z. L. Mei, J. Bai, T. M. Niu, and T. J. Cui, "A half Maxwell fish-eye lens antenna based on gradient-index metamaterials," *IEEE Trans. Antennas Propag.*, vol. 60, no. 1, pp. 398–401, Jan. 2012.
[22] C. T. Tai, "Maxwell fish-eye treated by Maxwell equations," *Nature*, vol. 182, no. 4649, pp. 1600–1601, Dec. 1958.
[23] M. Notomi, "Theory of light propagation in strongly modulated photonic crystals: Refraction like behavior in the vicinity of the photonic band gap," *Phys. Rev. B*, vol. 62, pp. 10 696–10 705, Oct. 2000. [Online]. Available: http://link.aps.org/doi/10.1103/PhysRevB.62.10696.
[24] E. Centeno and D. Cassagne, "Graded photonic crystals," *Opt. Lett.*, vol. 30, no. 17, pp. 2278–2280, Sep. 2005. [Online]. Available: http://ol.osa.org/abstract.cfm?URI=ol-30–17-2278.

[25] E. Akmansoy, E. Centeno, K. Vynck, D. Cassagne, and J.-M. Lourtioz, "Graded photonic crystals curve the flow of light: An experimental demonstration by the mirage effect," *Appl. Phys. Lett.*, vol. 92, no. 13, Art. no. 133501, 2008. [Online]. Available: http://scitation.aip.org/content/aip/journal/apl/92/13/10.1063/1.290168 4.
[26] E. Centeno, E. Akmansoy, K. Vynck, D. Cassagne, and J.-M. Lourtioz, "Light bending and quasi-transparency in metallic graded photonic crystals," *Photon. Nanostructures—Fundam. Appl.*, vol. 8, no. 2, pp. 120–124, 2010, special Issue {PECS} 8. [Online]. Available: http://www.sciencedirect.com/science/article/pii/S1569441009000546.
[27] F. Gadot, T. Brillat, E. Akmansoy, and A. de Lustrac, "New type of metallic photonic bandgap material suitable for microwave applications," *Electron. Lett.*, vol. 36, no. 7, pp. 640–641, Mar. 2000.
[28] A. Taflove and S. C. Hagness, *Computational Electrodynamics: The Finite-Difference Time-Domain Method, 2nd ed.* Norwood, MA, USA: Artech House Publishers, 2005.
[29] F. Gaufillet, "Cristaux photoniques à gradient: Dispositifs et applications," Ph.D. dissertation, Photonics Dept., Institut d'Électronique Fondamentale, Université Paris-Sud, Paris, 2014. [Online]. Available: https://tel.archives-ouvertes.fr/tel-01160435.
[30] F. Gaufillet and E. Akmansoy, "Graded photonic crystals for graded index lens," *Opt. Commun.*, vol. 285, no. 10/11, pp. 2638–2641, May 2012.
[31] F. Gaufillet and E. Akmansoy, "Design of flat graded index lenses using dielectric Graded Photonic Crystals," *Opt. Mater.*, vol. 47, pp. 555–560, Sep. 2015.
[32] F. Gaufillet and E. Akmansoy, "Graded Photonic Crystals for Luneburg Lens," *IEEE Photon. J.*, vol. 8, no. 1, Art no. 2400211, Feb. 2016.
[33] F. Gaufillet and É. Akmansoy, "Design and experimental evidence of a flat graded-index photonic crystal lens," *J. Appl. Phys.*, vol. 114, no. 8, Art no. 083105, 2013. [Online]. Available: http://scitation.aip.org/content/aip/journal/jap/114/8/10.1063/1.481736 8.
[34] F. Gaufillet, S. Marcellin, and E. Akmansoy, "Dielectric metamaterial-based gradient index lens in the terahertz frequency range," *IEEE J. Sel. Top. Quantum Electron.*, vol. 23, no. 4, Art no. 4700605, Jul./Aug. 2017.
[35] W. Jagger, "The optics of the spherical fish lens," *Vis. Res.*, vol. 32, no. 7, pp. 1271–1284, 1992. [Online]. Available: http://www.sciencedirect.com/science/article/pii/0042698992902225.
[36] C. Luo, S. G. Johnson, J. D. Joannopoulos, and J. B. Pendry, "Subwavelength imaging in photonic crystals," *Phys. Rev. B*, vol. 68, Art no. 045115, Jul. 2003. [Online]. Available: https://link.aps.org/doi/10.1103/PhysRevB.68.045115.